Available online at www.sciencedirect.com
SCIENCE DIRECT
Polymer 47 (2006) 5938–5945
polymer
www.elsevier.com/locate/polymer

Microstructural evolution of electrically activated polypropylene/layered silicate nanocomposites investigated by *in situ* synchrotron wide-angle X-ray scattering and dielectric relaxation analysis

Do Hoon Kim [a,1], Kwang Soo Cho [b], Tetsu Mitsumata [c], Kyung Hyun Ahn [a,*], Seung Jong Lee [a]

[a] *School of Chemical Engineering, Seoul National University, San 56-1 Shillim-dong, Seoul 151-744, Republic of Korea*
[b] *Department of Polymer Science, Kyungpook National University, Daegu 702-701, Republic of Korea*
[c] *Department of Polymer Science and Engineering, Yamagata University, Yonezawa 992-8510, Japan*

Received 24 April 2006; received in revised form 11 June 2006; accepted 14 June 2006
Available online 7 July 2006

Abstract

Electric field was found to facilitate the destruction of layer stacking and separation of silicate layers in polypropylene (PP)/layered silicate nanocomposites, resulting in the penetration of polymer chains into silicate galleries. In this study, we describe the real-time microstructural evolution of PP/clay nanocomposites under electric field investigated by *in situ* synchrotron wide-angle X-ray scattering (WAXS) analysis. We were able to identify two distinctive mechanisms for the formation of nanocomposites depending on the type of electric field. We observed that the exfoliation process prevails in the AC field, while the alignment of silicates parallel to the electric field predominates in the DC field. Dielectric relaxation analysis showed that the different mechanisms originate from different charge distributions of bound ions attached to the clay surfaces due to the applied electric field.

Keywords: Clay; Electric field; Nanocomposites

1. Introduction

It is well known that the addition of only a few percent of layered silicates can improve the material properties significantly compared to the conventional composites with micron-size fillers [1,2]. Several strategies have been proposed for the synthesis of nanocomposites, and the key issue lies in how to achieve good dispersion of the clays and how to control the degree of exfoliation of the layered silicates.

The application of this concept to polypropylene (PP)/clay nanocomposite is more challenging at least for two reasons. One is related to its impact on the market, while the other is technical. Since PP is widely used in many industries including automotives [2], its impact on the market cannot be overestimated. However, unlike the case of polyamide, PP does not include any polar group in its backbone and, consequently, it is difficult to obtain homogeneous dispersion of the silicate layers. Since Toyota group reported the formation of PP/clay hybrid composites by direct melt intercalation of montmorillonite (MMT) using maleic anhydride grafted PP (PP-*g*-MA) as a compatibilizer [3], PP/clay nanocomposites have been investigated by many researchers [3–5]. Even though exfoliated nanostructure can be obtained by this approach, the additives involved are expensive and need to be used in a significant amount, which prohibits the commercial application. Recently, several new chemical approaches have been reported to overcome these difficulties, by eliminating the need for the compatibilizer [6–8].

In addition to these chemical approaches, a novel physical approach that exploits electric field was proposed for the formation of PP/layered silicate nanocomposites [9]. With these

* Corresponding author.
E-mail address: ahnnet@snu.ac.kr (K.H. Ahn).
[1] Present address: Department of Chemical Engineering, University of Texas, Austin, TX 78712, USA.

0032-3861/$ - see front matter © 2006 Elsevier Ltd. All rights reserved.
doi:10.1016/j.polymer.2006.06.029

evidences, namely the increase in storage modulus with increasing exposure time to an electric field, the non-terminal behavior and drastic increase in the storage modulus at low frequency, the disappearance of the characteristic peak in X-ray diffraction after electric treatment, and the morphological changes, it was concluded that the electric field facilitates the destruction of layer stacking and separation of the silicate layers, resulting in the penetration of the polymer chains into the silicate galleries. However, precise mechanism of this effect has not been fully understood.

In this paper, we report the real-time wide-angle X-ray scattering (WAXS) experiments and dielectric relaxation analysis (DEA) of PP/layered silicate nanocomposites, with the purpose of understanding the mechanism on the formation of nanocomposites and the orientation of the layered silicates in the presence of electric field. We will identify two distinct mechanisms from WAXS analysis. One is the exfoliation process in AC electric field and the other is the alignment of the layered silicates in DC field. Through dielectric relaxation analysis, we will show these two different behaviors are closely related with the changes in charge distribution, especially with regard to the bound ions that are distributed on the layer surfaces in the presence of electric field.

2. Experimental section

PP ($M_w = 127{,}000$, $M_n = 13{,}000$, PolyMirae Corp.) and dimethyl hydrogenated-tallow ammonium modified MMT (Cloisite 20A, Southern Clay Products Inc.) were used in this study. The melt compounding of the PP/clay hybrid was performed in an intensive internal mixer (Haake Rheocord 90) at 50 rpm for 10 min after clay feeding at 180 °C. The weight fraction of Cloisite20A (C20A) was 5 wt%, and the corresponding samples are subsequently referred to as HP (Neat PP), HPC (PP with 5 wt% of clay), HPCA (treated under AC electric field), and HPCD (treated under DC electric field).

In situ synchrotron WAXS measurements were performed at the 4C2 beam line in the Pohang accelerator light source (PALS, Korea), which consists of 2 GeV linear accelerator (LINAC), storage ring, Si (111) double crystal monochromator, ion chambers, and two-dimensional CCD camera with 1042 pixels. The photon energy was set to 5.5 keV. WAXS patterns were recorded with a two-dimensional camera located at a distance of 22 cm from the sample. The detector can monitor up to 50 frames (1024 × 1024 pixels) at a rate of 40 s per 1 frame. AC of 1 kV/mm and 60 Hz, and DC of 1 kV/mm were applied with a function generator (Tektronix AFG 310) and high voltage amplifier (Trek 677B). The copper electrode was designed with a gap of 1.5 mm, height of 5.0 mm and width of 1.0 mm. The homogeneous electric field was applied perpendicular to the direction of the X-ray beam. No leakage current was detected.

The dielectric analyzer, DEA 2970 (TA instruments, Inc.) was used to estimate the dielectric properties such as permittivity, loss factor, and electric conductivity for electrically activated PP/clay nanocomposites under the isothermal condition of 190 °C. Each dielectric property was measured over the frequency range from 0.1 Hz to 10^5 Hz.

3. Results and discussion

Fig. 1 shows the result of time sweep test for PP/clay nanocomposites under AC (1 kV/mm-60 Hz) and DC (1 kV/mm) electric field. The storage modulus increases with time and

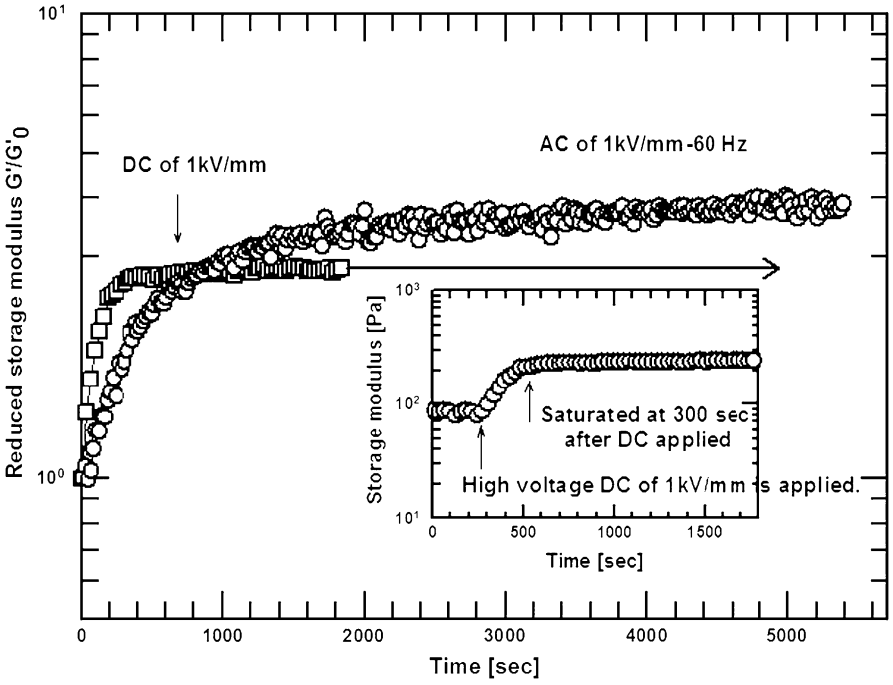

Fig. 1. Rheological properties of electrically activated polypropylene/clay nanocomposites under AC and DC electric fields. The experiments were carried out at the frequency of 1 rad/s and strain of 10%, which is linear region at 180 °C [9].

reaches a steady value as the AC electric field is applied. The increase in the storage modulus indicates the morphological evolution, that is, the layer-stacking destruction and separation of layered silicates [9]. Compared with that in AC electric field, the storage modulus becomes saturated much faster when DC electric field is applied. This means that the morphological changes in DC field is different from those in AC field. To verify the difference in its response under AC and DC fields, real-time WAXS experiments and DEA analysis will be carried out.

We first investigate the morphological changes in the layered silicates at 200 °C before applying the electric field. An isotropic ring pattern is observed, as shown in Fig. 2(A), which means that the layered silicates are dispersed randomly in polymer matrix. When the electric field is applied, the scattering pattern changes distinctively depending on the type of the electric field. In the AC field, the isotropic ring pattern becomes weaker and gets smaller and smaller as time goes on (not shown here in detail). This implies that layer-stacking destruction and separation of the layered silicates are progressing. In other words, the exfoliation process can be induced by applying AC electric field, which is also evidenced by other measurement techniques, including TEM, XRD and rheometry [9]. Snapshot (B) in Fig. 2 shows 2D WAXS pattern recorded 2385 s after the application of the electric field. In the DC field, the alignment of the layered silicates parallel to the electric field was observed at 318 s, which is shown in Fig. 2(C). These findings indicate the existence of two different mechanisms responsible for the formation of nanocomposites in the presence of AC and DC fields.

The time series of one-dimensional X-ray characteristic peaks of layered silicates recorded under AC field at 200 °C are shown in Fig. 2(a). In the WAXS experiment, only the electric field was applied on the contrary to the rheometry where both electric and flow fields were applied. The change in intensity of the intercalated and pristine diffraction peaks with time reflects the kinetics of the intercalation process, because the intensities of the pristine and intercalated basal reflections correspond to the concentrations of the unintercalated and intercalated silicates in the sample, respectively, under the assumption that the number of silicate layers remains the same during the intercalation process [10]. The initial d_{001} spacing of C20A is 3.0 nm at 200 °C and it shifts to a lower value of q in AC electric field. The position of the maximum peak, q_{max}, decreases as the exposure time increases. We note that the enhanced dispersion and exfoliation seems to follow three steps, which are depicted in Figs. 2(a) and 3(a).

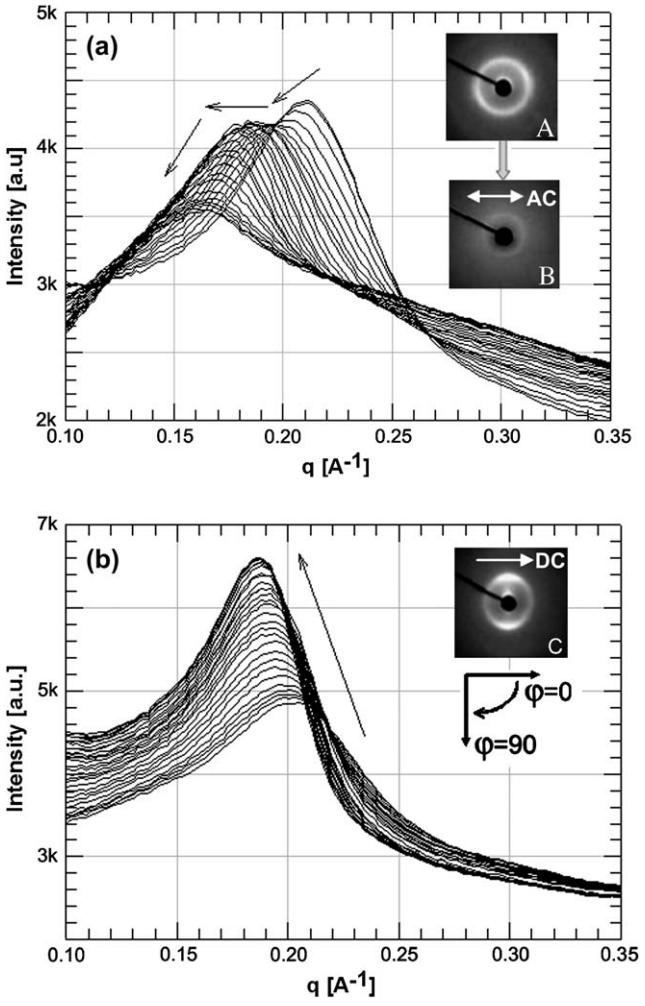

Fig. 2. One-dimensional characteristic peaks in AC (a) and DC (b) fields, and two-dimensional WAXS images: (A) initial state, (B) 2385 s after applying AC field and (C) 318 s after applying DC field.

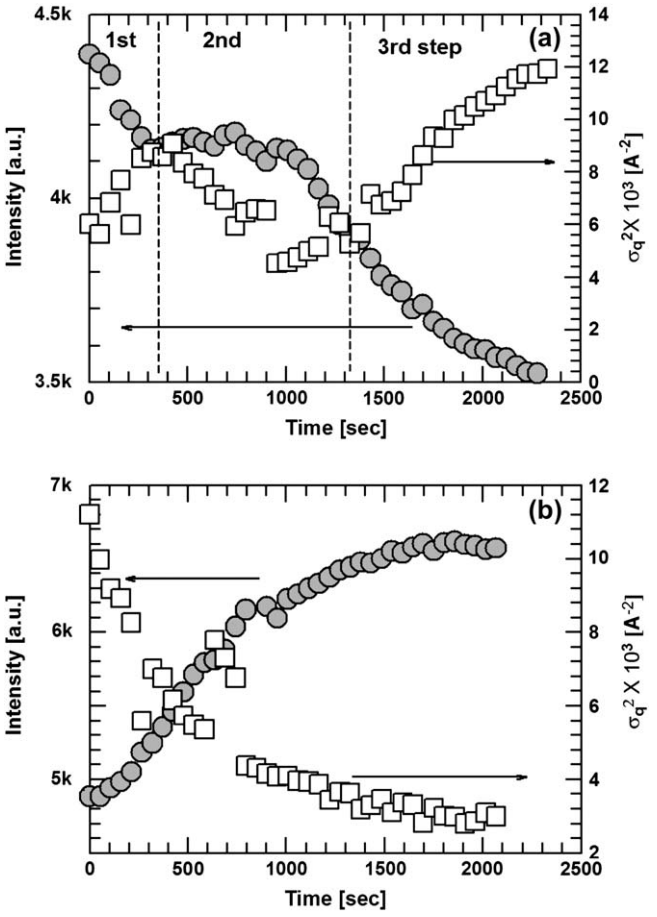

Fig. 3. Maximum intensity and full width half height in AC (a) and DC (b) fields.

In the first step, the maximum intensity, I_{max}, decreases as q_{max} decreases. The decrease in I_{max} is related to the decrease in the amount of silicate layers corresponding to q_{max}, while the decrease in q_{max} corresponds to an increase in the gallery spacing. The full-width at half-maximum (FWHM), σ_q^2, increases at this step, which implies the widening of the distribution of the gallery height. In the second step, I_{max} changes little but the value of q_{max} decreases with σ_q^2. This implies that the gallery height increases as the distribution narrows. In the third step, both I_{max} and σ_q^2 decrease with decreasing q_{max}. This implies there is a decrease in the number of layers in the clay stack caused by exfoliation. Therefore, the AC field causes exfoliation by disturbing (the first step) and rearranging (the second step) the gallery height distribution, leading to the gradual separation of the layers from the clay stacks (the third step). Under DC field, the morphological evolution is somewhat different. The isotropic ring pattern turns into two distinctive peaks at about $\varphi = 90°$ and $\varphi = 270°$, respectively, after the electric field is applied (see Fig. 2(C)). While the intensity of the isotropic ring pattern becomes weaker, that of the anisotropic pattern becomes stronger as time goes on and appears distinctively at 318 s. The anisotropic pattern implies that the orientation of the layered silicates has a preferred orientation, parallel to the electric field in this case. In contrast to the results obtained using AC field, the intensity of the characteristic peak increases with a slight shift of q_{max} to the left, which means that the intercalated silicates align themselves to the electric field (Fig. 2(b)). Furthermore, the maximum intensity in Fig. 3(b) increases gradually, even after the anisotropic pattern appears, and then reaches a steady value with a slight increase of basal spacing. The decrease of σ_q^2 means that a transition occurs from a disordered state into an ordered state, which can be understood by the increase in the alignment of the silicate layers parallel to the direction of the electric field.

Fig. 4 shows different morphologies of PP/clay nanocomposites after applying AC (1 kV/mm-60 Hz, 2385 s) and DC (1 kV/mm, 318 s) fields. While the destruction and random distribution of clay layers are observed under AC field (a), the orientation of clay tactoids parallel to the electric field can be found under DC field (b). The degree of orientation may well be quantified by the average orientation parameter, S_d, which can be defined using the Herman's orientation function [11–14];

$$S_d = \frac{3\langle \cos^2 \varphi \rangle - 1}{2}$$

where

$$\langle \cos^2 \varphi \rangle = \frac{\int_0^{2\pi} I(\varphi) \cos^2 \varphi \sin \varphi \, d\varphi}{\int_0^{\pi} I(\varphi) \sin \varphi \, d\varphi} \quad (1)$$

Here $I(\varphi)$ is the intensity at the azimuthal angle φ and the orientation parameters reported here are the averages of four orientation parameters calculated from each quadrant. The orientation parameter takes values of $S_d = 0$ and 1 for random orientation and perfect uniaxial orientation, respectively. Fig. 5 shows the orientation parameter for PP/clay nanocomposites under DC and AC fields. The orientation of clay tactoids rapidly increases with DC field and becomes saturated at about 0.58. The orientation parameter of the fully aligned system is typically between 0.6 and 0.7, and the value of 0.58 is comparable to the case of well-aligned low molecular weight nematic liquid crystals [13,14]. On the contrary, the orientation parameter does not change significantly in AC field but slightly decreases, which means the distribution of clay particles becomes more random as exfoliation progresses subjected to the AC field as discussed above.

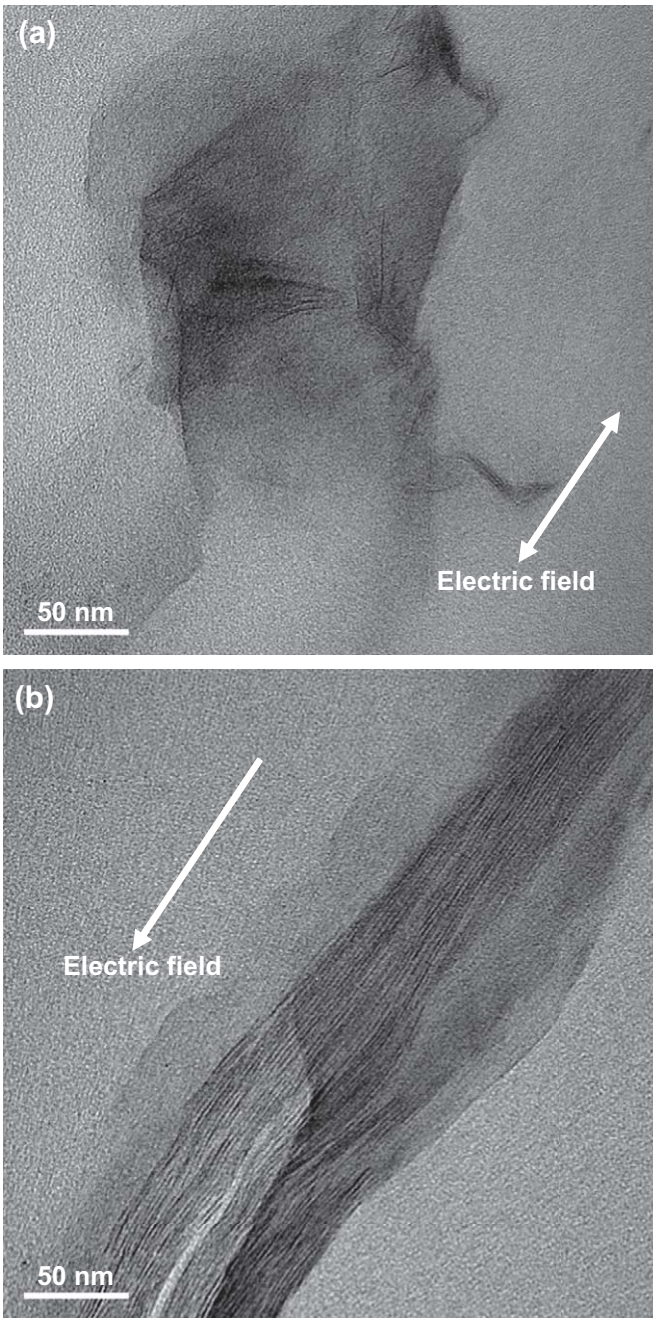

Fig. 4. TEM photographs of PP/clay nanocomposites after AC (1 kV/mm-60 Hz, 2385 s) (a) and DC field (1 kV/mm, 318 s) (b).

There are many studies on the orientation of silicate layers under flow field [12,15–18], but only a few on the orientation

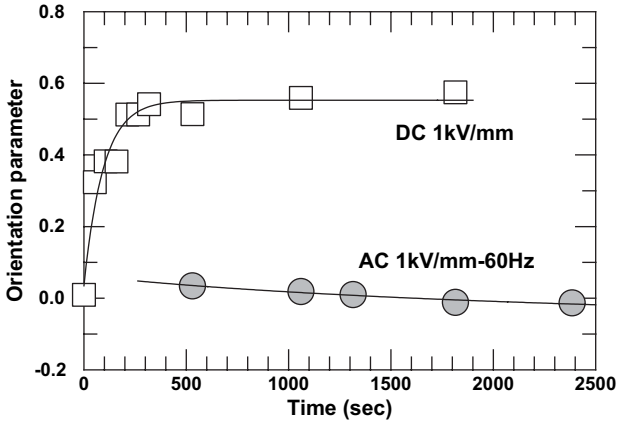

Fig. 5. Herman's orientation parameter, S_d, in AC and DC fields.

of the layered silicates under electric field [14,19,20]. They are in the form of electrorheological (ER) fluids [21,22], a kind of suspension in which conducting particles are suspended in a non-conducting medium such as mineral oil. Our system is unique in that the conducting particles are distributed in highly viscous polymer melt rather than mineral oil, which is much less viscous and the particles are easy to align and orient. The time scale for the layered silicates to align themselves parallel to the electric field can be estimated based on the simple polarization model [22],

$$t_s = \frac{\eta_s}{2\varepsilon_0 \varepsilon_s \beta^2 E^2} \tag{2}$$

where ε_0 is the permittivity of space and β is the effective polarizability defined as $(\varepsilon_r - 1)/(\varepsilon_r + 2)$ where $\varepsilon_r = \varepsilon_p/\varepsilon_s$; ε_p and ε_s are the dielectric constants of particles and that of suspending medium, respectively. E and η_s are the applied electric field and the viscosity of solution, respectively. In general, the time scale for the alignment of typical ER fluid is of the order of a few milliseconds. As $\varepsilon_s = 2.5$, $\varepsilon_p = 4.2$, $\varepsilon_0 = 8.85 \times 10^{-12}$ F/m, $\beta = 0.25$, $E = 1000$ V/mm, $\eta_s = 800$ Pa, in this case, the time scale for the alignment of the layered silicates under DC field is about 288 s. This seems to be reasonable because the mobility of the clay in this case is restricted by the highly viscous matrix. The calculated value of t_s is in good agreement with the experimental results of the WAXS measurements as well as the rheological measurements. The bright strings in 2D WAXS images become distinct in this time scale (between 200 and 318 s) and the orientation parameter reaches a saturation value at this time scale as well. The storage modulus also saturates at the same time scale in DC field (see Fig. 1). This means that the clays respond to DC field in the same way as ER fluids do, and that the silicate layers or their clusters align themselves to the direction of the electric field.

To understand the mechanism under AC field, dielectric relaxation analysis is carried out, that provides information on the molecular mobility in polymer melts and, particularly the information on the behavior of the ions on the clay surface in this case. The electric conductivity of HP is in the order of

Table 1
Electric conductivity and dielectric properties with and without electric fields

Sample code	$\sigma_{0.1}$ [a]	σ_{100k} [b]	ε'_0 [c]	ε'_∞ [d]	β [e]	τ [f]	N_b [g]
HP	3.38	9.69	–	–	–	–	–
HPC	10.7	254	2.72	2.44	0.45	0.049	50.6
HPCA	13.9	358	3.33	2.65	0.39	0.50	12.0
HPCD	16.8	301	2.76	2.40	0.45	0.065	49.0

[a] Electric conductivity at 0.1 Hz ($\times 10^{-12}$ S/cm).
[b] Electric conductivity at 100 kHz ($\times 10^{-9}$ S/cm).
[c] Real part of dielectric constant at low frequency used in Eq. (8).
[d] Real part of dielectric constant at high frequency used in Eq. (8).
[e] Broadness of the distribution of the relaxation time.
[f] Mean relaxation time (ms).
[g] Number of bound ions, $\varepsilon_0 \Delta\varepsilon'/\tau$ ($\times 10^{-9}$ S/m).

10^{-12}–10^{-9} S/cm, which is typical of an insulator (Table 1). The electric conductivities of HPC, HPCA and HPCD are in the range of 10^{-9}–10^{-7} S/cm, that is 1–2 orders of magnitude higher than that of HP. This suggests that PP/clay has a large amount of carriers contributing to the electric conductivity. These carriers would be surfactant ions originating from the clays [23–25].

The complex dielectric constant ε^* is defined as

$$\varepsilon^* = \varepsilon' - i\varepsilon'' \tag{3}$$

where ε' and ε'' stand for the real and imaginary parts of the complex dielectric constant, respectively. The real part of the complex dielectric constant ε' is shown in Fig. 6(a). ε' of HP slightly decreases below 6 rad/s and becomes independent of frequency above 6 rad/s. ε' of HPC decreases below 6 rad/s and reaches a plateau in the frequency range between 6 rad/s and 60 rad/s, after which it gradually decreases with frequency. The decrease in ε' below 10 rad/s can be attributed to the electrode polarization effect. On the other hand, the decrease in ε' above 10^3 rad/s is considered as the dielectric relaxation of the ions. To figure out the dielectric relaxation of the ions in PP/clay melts, the electrode polarization, which is the contribution of electrode screening and conductivity effects in low-frequency region under the action of the applied electric field (1.0 V) in DEA measurements, was subtracted from as measured ε'. The as measured ε' can be decomposed by two contributions; one from electrode polarization ε'_{el} and the other from relaxation ε'_{relax}.

$$\varepsilon' = \varepsilon'_{el} + \varepsilon'_{relax} \tag{4}$$

The contribution of electrode polarization to the real part of the dielectric constant is known to have a power relation with frequency [26,27]

$$\varepsilon'_{el} = \alpha\omega^{-3/2} \tag{5}$$

Here, α is a constant, ω stands for the frequency of the electric field. By assuming $\alpha = \varepsilon'_{0.1Hz}\ \omega^{3/2}_{0.1Hz}$, the electrode polarization term was evaluated. The real part of the dielectric constant due to the relaxation of the ions is shown in Fig. 7(a). No dielectric relaxation occurs in PP without clay although small increment in ε'_{relax} is observed at high frequency end. On the contrary, the dielectric relaxation is observed in

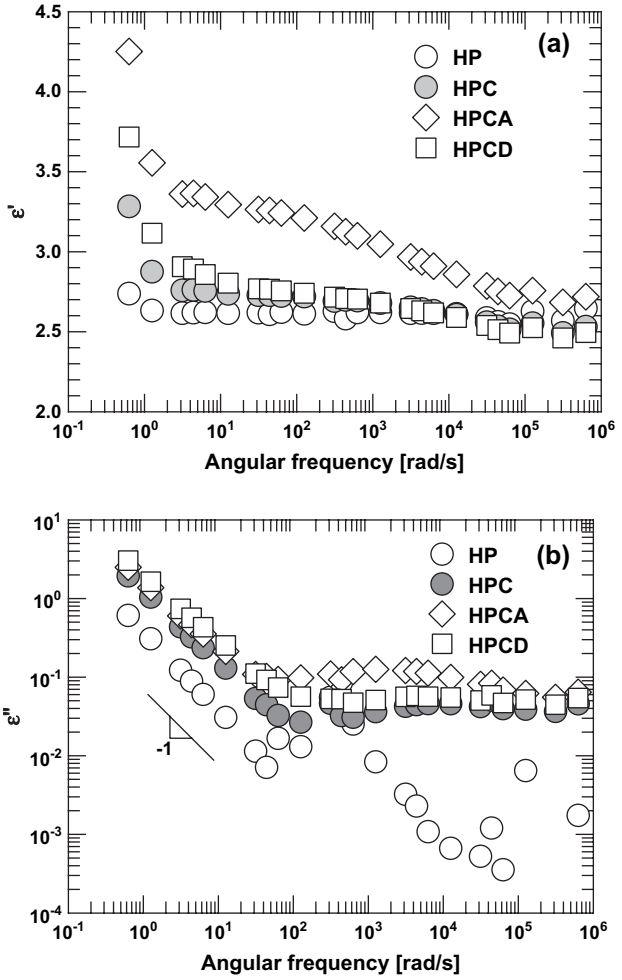

Fig. 6. Frequency dependence of the real part (a) and imaginary part (b) of the dielectric constants at 190 °C.

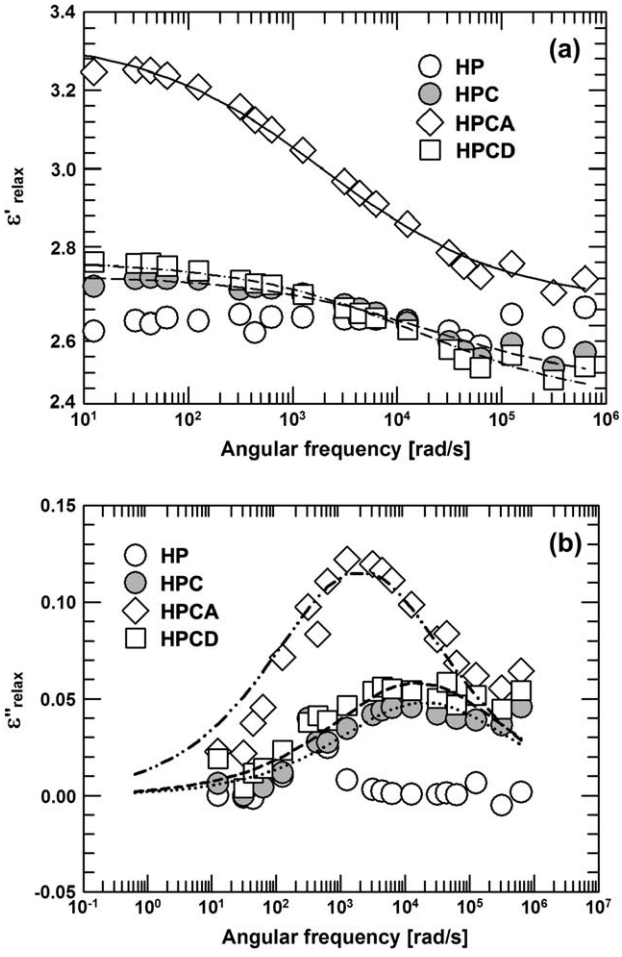

Fig. 7. Frequency dependence of the real part (a) and imaginary part (b) of the dielectric constants after subtracting the electrode polarization term.

HPC, HPCA, and HPCD. This strongly suggests that the dielectric relaxation observed in this frequency regime is attributed to the relaxation of the ions in the clay. A clear difference between these samples is the dielectric increment. HPCA demonstrates a large dielectric relaxation compared to the others. The dielectric increment of HPCD is as large as that of HPC.

The imaginary part of the complex dielectric constant ε'' is shown in Fig. 6(b). At low frequency, ε'' decreases for all the samples by a power of frequency, suggesting the electrode polarization effect. The imaginary part of the dielectric constant can be decomposed into the term due to relaxation and the DC-conductivity originating from the electrode polarization:

$$\varepsilon'' = \varepsilon''_{\text{relax}} + \varepsilon''_{\text{DC}} \tag{6}$$

According to the theory of dielectrics, the DC-conductivity term can be simplified as

$$\varepsilon''_{\text{DC}} = \frac{\sigma_{\text{DC}}}{\omega} \tag{7}$$

where σ and ω are the DC-conductivity and frequency, respectively. We use this empirical equation to estimate the relaxation contribution by subtracting the DC-conductivity term from the as measured ε''. Fig. 7(b) shows the relaxation contribution of ε''. A pronounced peak is observed in HPCA and comparatively weak peaks in HPC and HPCD. HP does not show any peak in the frequency range we are interested in. The relaxation can be fitted with the theoretical equations, which are often referred to as the Cole–Cole's circular arc law [26,27],

$$\varepsilon'_{\text{relax}} = \varepsilon'_{\infty} + \frac{\varepsilon'_0 - \varepsilon'_{\infty}}{2}\left[1 - \frac{\sinh \beta x}{\cosh \beta x + \cos(\pi\beta/2)}\right],$$
$$\varepsilon''_{\text{relax}} = \frac{\varepsilon'_0 - \varepsilon'_{\infty}}{2}\frac{\sinh \beta x}{\cosh \beta x + \cos(\pi\beta/2)} \tag{8}$$

where $x = \ln \omega\tau_0$, and ω is the angular frequency of the applied electric field, τ_0 is the mean relaxation time, and β stands for the parameter representing the broadness of the distribution of the relaxation times. Nonlinear least mean squares fitting was carried out and the results are presented in Table 1 and in Fig. 7 as dotted lines. As can be seen in Table 1, the β value of HPCA is much lower than that of HPC and HPCD, suggesting that there is a wide distribution of the relaxation times

under AC field, which is far from Debye type relaxation. The relaxation time of HPCA is longer than those of HPC and HPCD, and the relaxation peak of HPCA is much higher than those of HPC and HPCD. Moreover, the peak frequency is in the order HPCA < HPCD < HPC, which coincides with the order determined by Eq. (8). The decreased peak frequency is related with the increased amount of layered silicate surface area as a result of the increased degree of exfoliation as discussed by Davis et al [23].

We now analyze the mobility of the ions based on the theory of dielectrics. Ions in the melts can be divided into two types. One is free ion (cationic surfactants in polymer matrix) which contributes to the electric conductivity, and the other is bound ion (cationic surfactants on clay surface) which contributes to the dielectric relaxation. We consider the behavior of the bound ions attached to the clay surface. The number density of the bound ions can be obtained by the following relations [23–25,28]. The relaxation time τ can be determined by the equation

$$\tau = \frac{L^2}{D} \tag{9}$$

Here, L and D represent the diffusion length and the diffusion constant of the bound ions, respectively. As mentioned above, the relaxation time and the dielectric increments of HPCA are larger than those of HPC and HPCD. The dielectric increment $\Delta\varepsilon$ is expressed as

$$\Delta\varepsilon = \frac{\alpha_e N_b}{\varepsilon_0} \tag{10}$$

Here N_b is the number density of the bound ions in the melts and α_e is the electrical polarizability due to a bound ion given by

$$\alpha_e \sim \frac{e^2 L^2}{kT} \tag{11}$$

where e is the elementary charge, k and T are Boltzmann constant and temperature, respectively. The following relation between the number density of the bound ions and the dielectric increment can be obtained using Eqs. (9–11)

$$\frac{\varepsilon_0 \Delta\varepsilon}{\tau} \propto N_b \tag{12}$$

The estimated values of N_b are listed in Table 1. The number density of the bound ions, N_b, of HPCA is much smaller than those of HPC and HPCD, even though HPCA has as many free ions as HPC and HPCD. From these observations, it will be natural to think that the number density of the bound ions is related to the increase in the degree of exfoliation under AC field. While the PP/clay composites have a large amount of free ions and bound ions after melt compounding (HPC), the PP/clay nanocomposites electrically activated under AC field (HPCA) have a smaller number of bound ions. This implies the transformation of bound ions into free ions, due to the dissociation of the bound ions in the presence of AC electric field. The dissociation of the bound ions indicates there is a change in the charge distribution on the clay surface, which causes an imbalance between the van der Waals attraction and the electrostatic repulsion. When the electrostatic repulsive force overcomes the attractive van der Waals force between the layers, they repel each other resulting in the destruction of layer stacking. On the other hand, we note the role of non-bound ions dissociated from the clay surface. The dissociation of ions from the clay surface causes the collapse of clay layers by thermal degradation [29,30] or the diffusion into polymer matrix during melt processing [31] opposite to the observation of this study. In these cases, there are no external driving forces like electric field. The other possibility is the screening effect from dissociated ions. The non-bound ions would screen the applied electric field and weaken the local field acting on the clay surface, thereby suppressing the exfoliation to some extent. Important is the balance between the forces, i.e., electrostatic repulsion and van der Waals attraction as we mentioned above. If the screening effect is dominant, the exfoliation process may not proceed so far. However, the exfoliation process under strong AC electric field was significant as evidenced from our observation; from WAXS, TEM and rheology. Therefore, we believe that the screening effect by non-bound ions is negligible in this study. From these reasons, the layer-stacking destruction and separation of the silicate layers arise from this imbalance between the two forces in strong AC electric field. On the other hand, the N_b value of HPCD does not change, which means that the electrostatic balance does not vary significantly under DC field. In this case, the stacks of clay layers are not dissociated but align to the field direction like anisotropic particles as in the case of ER fluids.

4. Conclusions

We demonstrated the existence of two distinctive mechanisms of electrically activated polymer layered silicate nanocomposites under AC and DC electric fields for the first time using real-time synchrotron WAXS measurements, dielectric relaxation analysis and rheology. The exfoliation process prevails in the AC field due to the imbalance between the van der Waals attraction and the electrostatic repulsion originating from the dissociation of the bound ions from the clay surfaces. On the other hand, the alignment of the silicate layers parallel to the electric field prevails in the DC field as in the case of typical ER fluids. The time scale of this alignment process, calculated by means of the simple polarization model, is in good agreement with the experimental results. This means that we can regulate the degree of exfoliation (or intercalation) and alignment of the layered silicates by controlling both the applied electric field and the flow field.

Acknowledgement

The authors wish to acknowledge the Korea Energy Management Corporation (KEMCO) for the financial support through the project No. 2005-R-NM01-P-01-2-400-2005.

The X-ray experiments performed at the 4C2 beam line at the Pohang Light Source were supported in part by the Korean Ministry of Science and Technology (MOST) and in part by the Pohang Iron and Steel Co.

References

[1] Giannelis EP. Adv Mater 1996;8:29.
[2] Collister J. Polymer nanocomposites: synthesis, characterization, and modeling. In: Vaia RA, Krishnamoorti R, editors. London: Oxford university press; 2002 [chapter 2].
[3] Kato M, Usuki A, Okada A. J Appl Polym Sci 1997;66:1781.
[4] Gagali G, Ramesh C, Lele A. Macromolecules 2001;34:852.
[5] Solomon MJ, Almusallam AS, Seefeldt KF, Somwangthanaroj A, Varadan P. Macromolecules 2001;34:1864.
[6] Liu X, Wu Q. Polymer 2001;42:10013.
[7] Tjong SC, Meng YZ, Hay AS. Chem Mater 2002;14:44.
[8] Sun T, Garces JM. Adv Mater 2002;14:128.
[9] Kim DH, Park JU, Ahn KH, Lee SJ. Macromol Rapid Commun 2003; 24:388.
[10] Vaia RA, Jandt KD, Kramer EJ, Giannelis EP. Macromolecules 1995; 28:8080.
[11] Ugaz VM, Burghardt WR. Macromolecules 1998;31:8474.
[12] Lele A, Mackley M, Gagali G, Ramesh C. J Rheol 2002;46:1091.
[13] Koerner H, Luo Y, Li X, Cohen C, Hedden RC, Ober CK. Macromolecules 2003;36:1975.
[14] Koerner H, Jacobs D, Tomlin DW, Busbee JD, Vaia RD. Adv Mater 2004;16:297.
[15] Ren J, Barbara FC, Mitchell CA, Krishnamoorti R. Macromolecules 2003;36:4188.
[16] Bafna A, Beaucag G, Mirabella F, Mehta S. Polymer 2003;44:1103.
[17] Schmidt G, Nakatani AI, Butler PD, Karim A, Han CC. Macromolecules 2000;33:7219.
[18] Okamoto M, Nam PH, Maiti P, Kotaka T, Hasegawa N, Usuki A. Nano Lett 2001;1:295.
[19] Kim JW, Noh MH, Choi HJ, Lee DC, Jhon MS. Polymer 2000;41:1229.
[20] Lim YT, Park JH, Park O. J Colloid Interface Sci 2002;245:198.
[21] See H. Kor-Aust Rheol J 1999;11:169.
[22] Larson RG. The structure and rheology of complex fluids. New York: Oxford university press; 1999 [chapter 8].
[23] Davis RD, Bur AJ, McBrearty M, Lee Y-H, Gilman JW, Start PR. Polymer 2004;45:6487.
[24] Noda N, Lee Y-H, Bur AJ, Prabhu VM, Snyder CR, Roth SC, et al. Polymer 2005;46:7201.
[25] Bur AJ, Lee Y-H, Roth SC, Start PR. Polymer 2005;46:10908.
[26] Cole KS, Cole RH. J Chem Phys 1941;9:341.
[27] Scheider W. J Phys Chem 1975;79:127.
[28] Neelakanta PS. Handbook of electromagnetic materials: monolithic and composite versions and their applications. New York: CRC press; 1995 [chapter 2].
[29] Lee D, Char K. Polym Degrad Stab 2002;75:555.
[30] Gelfer M, Burger C, Fadeev A, Sics I, Chu B, Hsiao BS, et al. Langmuir 2004;20:3746.
[31] Shah RK, Paul DR. Polymer 2006;47:4075.